Numerical and experimental investigations of the effective thermal conductivity of snow

N. Calonne,[1] F. Flin,[1] S. Morin,[1] B. Lesaffre,[1] S. Rolland du Roscoat,[2] and C. Geindreau[2]

[1] We carried out numerical simulations of the conductivity of snow using microtomographic images. The full tensor of the effective thermal conductivity ($\mathbf{k}_{\mathrm{eff}}$) was computed from 30 three-dimensional images of the snow microstructure, spanning all types of seasonal snow. Only conduction through ice and interstitial air were considered. The obtained values are strongly correlated to snow density. The main cause for the slight scatter around the regression curve to snow density is the anisotropy of $\mathbf{k}_{\mathrm{eff}}$: the vertical component of $\mathbf{k}_{\mathrm{eff}}$ of facetted crystals and depth hoar samples is up to 1.5 times larger than the horizontal component, while rounded grains sampled deeply in the snowpack exhibit the inverse behavior. Results of simulations neglecting the conduction in the interstitial air indicate that this phase plays a vital role in heat conduction through snow. The computed effective thermal conductivity is found to increase with decreasing temperature, mostly following the temperature dependency of the thermal conductivity of ice. The results are compared to experimental data obtained either with the needle-probe technique or using combined measurements of the vertical heat flux and the corresponding temperature gradient. Needle-probe measurements are systematically significantly lower than those from the two other techniques. The observed discrepancies between the three methods are investigated and briefly discussed. **Citation:** Calonne, N., F. Flin, S. Morin, B. Lesaffre, S. Rolland du Roscoat, and C. Geindreau (2011), Numerical and experimental investigations of the effective thermal conductivity of snow, *Geophys. Res. Lett.*, *38*, L23501, doi:10.1029/2011GL049234.

1. Introduction

[2] Snow on the ground is a complex porous medium made of air and up to three phases of water (ice, water vapor and liquid water). Understanding heat and mass transfer through the snowpack is critical to assess the climatic and hydrological role of snow in the cryosphere. It is also needed to predict morphological changes in snow crystals [*Brzoska et al.*, 2008; *Flin and Brzoska*, 2008; *Kaempfer and Plapp*, 2009; *Pinzer and Schneebeli*, 2009], the vertical distribution of which governs, for example, the surface energy balance and the mechanical stability of the snowpack [*Armstrong and Brun*, 2008].

[3] Heat transfer through snow proceeds by conduction through ice and air, but is also potentially affected by phase change effects, water vapor diffusion and air convection in the pores [*Arons and Colbeck*, 1995; *Sturm et al.*, 1997]. Defining in a physically sound manner the thermal conductivity of snow, i.e., the tensor ($\mathbf{k}$) linking the macroscopic temperature gradient (∇T) and the heat flux ($\mathbf{F}$) through the Fourier's law ($\mathbf{F} = -\mathbf{k}\nabla T$), is thus challenging because conductive and nonconductive processes both contribute to heat transfer through snow. From experimental relationships between ∇T and $\mathbf{F}$, many investigators have derived an apparent thermal conductivity $k^{\star}$, which in general is treated as a scalar, $k^{\star}$, either assuming the medium to be isotropic, or at most focusing on its vertical component [*Yen*, 1981; *Sturm et al.*, 1997; *Kaempfer et al.*, 2005; *Morin et al.*, 2010; *Riche and Schneebeli*, 2010].

[4] To meet the needs of applications that require the thermal properties of snow to be estimated based on other physical variables (e.g., numerical snowpack models), experimental fits between $k^{\star}$ and snow density (ρ) have been proposed [*Yen*, 1981; *Sturm et al.*, 1997; *Domine et al.*, 2011]. Such regression curves differ widely: there is up to a factor of two difference between the regression curve of *Sturm et al.* [1997] and *Yen* [1981]. In addition, a considerable scatter of measured $k^{\star}$ values is found around the best fitting curve between $k^{\star}$ and ρ [*Sturm et al.*, 1997]. Both of these issues highlight the need for a re-assessment of the variables related to $k^{\star}$, the partitioning between the various physical processes involved in heat transfer, and the experimental methods used to infer $k^{\star}$.

[5] To contribute to this effort, we carried out numerical simulations of the conductivity of snow from its microstructure. This was done using 30 different 3D images of snow obtained by means of microtomography [*Brzoska et al.*, 1999; *Coléou et al.*, 2001; *Schneebeli and Sokratov*, 2004; *Kaempfer et al.*, 2005]. Only conduction through ice and air was considered in the heat transfer, leading to computing the true effective thermal conductivity tensor of snow ($\mathbf{k}_{\mathrm{eff}}$) from a material science perspective [*Rolland du Roscoat et al.*, 2008]. This work follows the pioneering developments of *Kaempfer et al.* [2005], who first reported computations of the vertical component of $\mathbf{k}_{\mathrm{eff}}$ from tomographic images and compared them to experimental data. The main differences lie in the fact that our study considers a wide range of snow types, uses the periodic homogenization method [*Auriault et al.*, 2009] and evaluates the anisotropy of $\mathbf{k}_{\mathrm{eff}}$. In addition, it includes thermal conduction in interstitial air, which was neglected by *Kaempfer et al.* [2005] and, more recently, by *Shertzer and Adams* [2011].

2. Methods

2.1. Snow Samples

[6] The numerical analyses were performed on 30 tomographic 3D images obtained from previous experiments or

[1]CEN, CNRM-GAME, URA 1357, Météo-France–CNRS, Saint Martin d'Hères, France.
[2]3S-R UMR 5521, Université Joseph Fourier Grenoble 1–Grenoble INP–CNRS, Grenoble, France.

field sampling, spanning most snow types of seasonal snow, i.e., Precipitation Particles (PP), Decomposing and Fragmented precipitation particles (DF), Rounded Grains (RG), Faceted Crystals (FC), Depth Hoar (DH) and Melt Forms (MF), according to the International Classification for Seasonal Snow on the Ground (ICSSG) [*Fierz et al.*, 2009]. Most snow samples were impregnated with 1-chloronaphthalene prior to 3D imaging, as described by *Flin et al.* [2003]. A few other samples were prepared using a previously developed technique (diethyl-orthophthalate soaking, followed by iso-octane rinsing just before tomography [*Coléou et al.*, 2001]).

[7] One third of the snow samples were directly collected in the field: 10 snow specimens (PP, DF and RG) were sampled at increasing depths in the snowpack of the Girose glacier (Écrins, French Alps) [*Flin et al.*, 2011]. Another PP snow sample was collected at Col de Porte (Chartreuse, French Alps). The remaining snow samples were obtained during controlled cold-room experiments: a first series (PP, DF and RG) was obtained under isothermal conditions at 271 K directly from deposited natural snow [*Flin et al.*, 2004]. Another sample (RG) was obtained under similar conditions, but after sieving. Four samples were obtained from different experiments where the snow evolved under a fixed temperature gradient ranging between 16 and 100 K m^{-1}, at a temperature between 268 and 270 K. These specimens correspond to various stages of transformations into facetted crystals and depth hoar [*Coléou et al.*, 2001; *Flin and Brzoska*, 2008]. A series of wet snow samples (MF) were obtained by grain coarsening in water-saturated snow using the method of *Raymond and Tusima* [1979] followed by draining of their liquid water content [*Coléou et al.*, 2001; *Flin et al.*, 2011]. Additional information concerning the samples is provided in the auxiliary materials.[1]

2.2. Computation of the Effective Thermal Conductivity of Snow

[8] Let us consider heterogeneous systems such as porous media where l and L are the characteristic lengths of the heterogeneities at the pore scale and of the macroscopic sample or excitation, respectively. Physical phenomena in such systems can be modeled by an equivalent continuous macroscopic description, provided that the condition of separation of scales is satisfied [*Auriault*, 1991; *Auriault et al.*, 2009], i.e., L is sufficiently large compared to l. This condition implies the existence of a Representative Elementary Volume (REV) of size l for the material. We provide here the main steps concerning the derivation of the macroscopic heat transfer equation from the physics at the pore scale using the homogenization method for periodic structures [*Bensoussan et al.*, 1978; *Auriault*, 1991].

[9] Without loss of generality, the medium is assumed to be Ω-periodic. The period, i.e., the REV, is defined by Ω, where Ω_{ice} and Ω_{air} are the domains occupied by the ice and the air respectively. The common boundary of Ω_{ice} and Ω_{air} is denoted Γ. The size of the periodic cell Ω is l.

Neglecting convection, phase change and under steady state conditions, heat transfers at the microscopic scale are described by:

$$\nabla \cdot (k_{ice} \nabla T_{ice}) = 0 \quad \text{in } \Omega_{ice} \tag{1}$$

$$\nabla \cdot (k_{air} \nabla T_{air}) = 0 \quad \text{in } \Omega_{air} \tag{2}$$

$$T_{ice} - T_{air} = 0 \quad \text{on } \Gamma \tag{3}$$

$$(k_{air} \nabla T_{air} - k_{ice} \nabla T_{ice}) \cdot \mathbf{n} = 0 \quad \text{on } \Gamma \tag{4}$$

where $\mathbf{n}$ is the normal to Γ. T refers to the temperature and k to the thermal conductivity (considered isotropic) of the phases denoted in subscripts. Using the homogenization method for periodic structures, it can be shown that the corresponding macroscopic description is [*Auriault et al.*, 2009]:

$$\nabla \cdot (\mathbf{k}_{eff} \nabla T) = 0, \tag{5}$$

where $\mathbf{k}_{eff}$ is the effective thermal conductivity tensor defined as:

$$\mathbf{k}_{eff} = \frac{1}{|\Omega|} \left(\int_{\Omega_{air}} k_{air} (\nabla \mathbf{t}_{air} + \mathbf{I}) d\Omega + \int_{\Omega_{ice}} k_{ice} (\nabla \mathbf{t}_{ice} + \mathbf{I}) d\Omega \right) \tag{6}$$

where $\mathbf{I}$ is the identity tensor, and where the two Ω-periodic vectors $\mathbf{t}_{ice}$ and $\mathbf{t}_{air}$ are solutions of the following boundary value problem over the REV:

$$\nabla \cdot (k_{ice} (\nabla \mathbf{t}_{ice} + \mathbf{I})) = \mathbf{0} \quad \text{in } \Omega_{ice} \tag{7}$$

$$\nabla \cdot (k_{air} (\nabla \mathbf{t}_{air} + \mathbf{I})) = \mathbf{0} \quad \text{in } \Omega_{air} \tag{8}$$

$$\mathbf{t}_{ice} - \mathbf{t}_{air} = \mathbf{0} \quad \text{on } \Gamma \tag{9}$$

$$(k_{air} (\nabla \mathbf{t}_{air} + \mathbf{I}) - k_{ice} (\nabla \mathbf{t}_{ice} + \mathbf{I})) \cdot \mathbf{n} = \mathbf{0} \quad \text{on } \Gamma \tag{10}$$

$$\frac{1}{|\Omega|} \int_{\Omega} (\mathbf{t}_{air} + \mathbf{t}_{ice}) d\Omega = \mathbf{0} \tag{11}$$

In what follows, this boundary value problem has been numerically solved on REVs extracted from 3D images of snow by using the commercial software Geodict [*Thoemen et al.*, 2008].

[10] Computations were carried out for all samples using the thermal properties of ice and air at 271 K ($k_{air} = 0.024$ W m^{-1} K^{-1} and $k_{air} = 2.107$ W m^{-1} K^{-1}). Computations were also carried out for a few selected samples, using thermal properties of ice and air at 203 K, i.e., k_{air} and k_{ice} values are 0.019 W m^{-1} K^{-1} and 2.900 W m^{-1} K^{-1}, respectively [*Yen*, 1981; *Sturm et al.*, 1997]. Finally, calculations were also performed for some samples, neglecting conduction in air, i.e., setting $k_{air} = 0$ W m^{-1} K^{-1}. We refer to k_{eff} as the average value of the three diagonal terms of
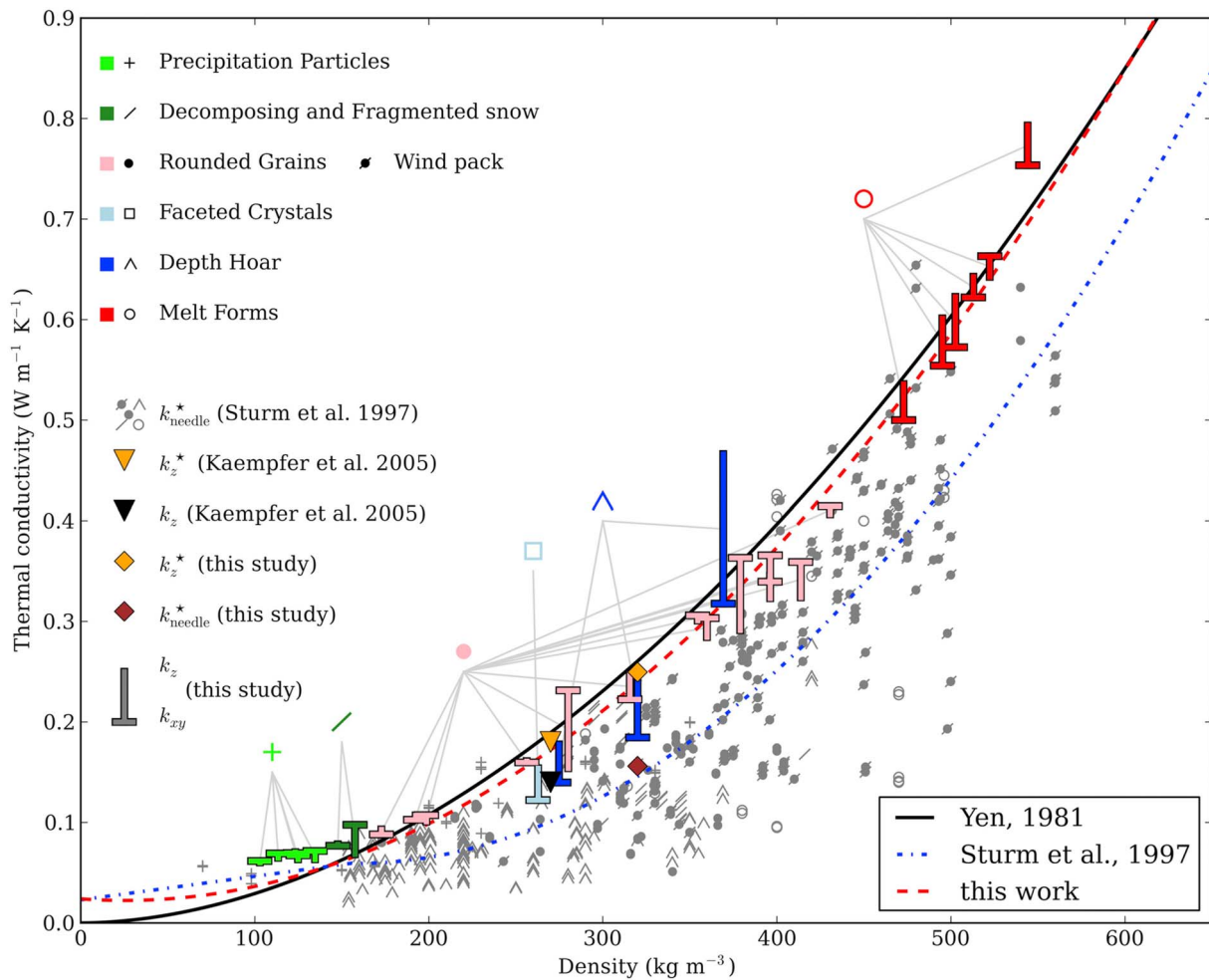
Figure 1. Effective thermal conductivity vs. snow density (ρ). The k_z and k_{xy} components of the computed $\mathbf{k}_{eff}$ data are provided ("T" shape symbols pointing to the k_z value) and compared to (i) needle-probe measurements by *Sturm et al.* [1997], using gray symbols corresponding to the ICSSG [*Fierz et al.*, 2009], (ii) numerical and experimental data from *Kaempfer et al.* [2005] using inverted triangles in black and yellow, respectively and (iii) experimental data from this study using diamonds. Also shown are the regression curves from *Yen* [1981], *Sturm et al.* [1997] and the quadratic equation derived in this study. See text for a full description of the notations used.

$\mathbf{k}_{eff}$, k_z its vertical component, and k_{xy} the average of its two horizontal components.

2.3. Computation of Other Variables From 3D Images

[11] The representative elementary volume (REV) constitutes the smallest fraction of the sample volume from which a variable representative of the whole can be determined. For all snow samples, attention was paid to ensure that computations of the thermal conductivity and the density were carried out on a REV. It can be estimated by calculating values of a given variable from several subvolumes of increasing sizes. The REV is reached as soon as values do not vary significantly when sub-volumes of computation increase. Note that the REV size depends on the variable and on the sample studied. For the considered study, REVs for thermal conductivity estimation range from about 2.5 mm (PP) to 5.5 mm (MF). Calculations performed on a lower volume than the REV were disregarded. Snow density was estimated from the tomographic images using a standard voxel counting algorithm.

2.4. Experimental Data

[12] In parallel to the numerical experiments described above, an experiment was carried out to compare thermal conductivities obtained numerically to those measured experimentally on the same samples. A snow slab (area: 1 m^2, thickness: 0.14 m) was exposed in a cold room to a high vertical temperature gradient (43 K m^{-1}) maintained by two horizontal copper plates thermally regulated at 272 and 266 K, at the bottom and top, respectively. The experiment lasted for three weeks, during which the snow, originally sieved rounded grains with a density of 300 kg m^{-3}, transformed into depth hoar, with an insignificant change in density. Two of the snow samples used for numerical computations originate from this experiment. In addition, the thermal conductivity of snow was measured using a needle-probe following the method of *Morin et al.* [2010]. Briefly, a needle (Hukseflux TP02) with a diameter of 1.5 mm and a heated length of 10 cm was inserted in the snow at half-height and remained there for the whole experiment.
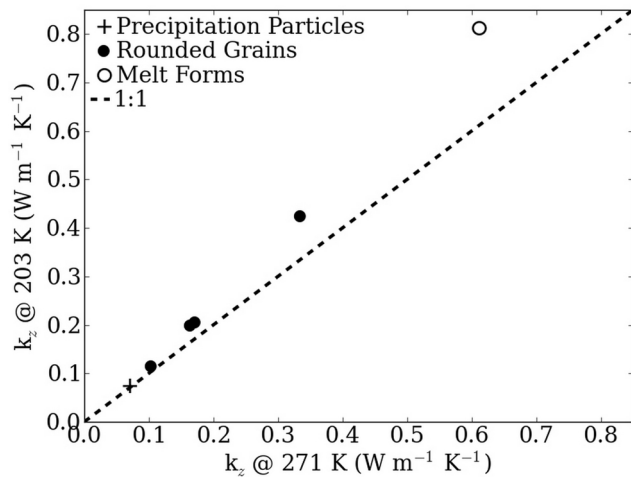
Figure 2. Impact of temperature on the effective thermal conductivity of snow. Computations were made using the thermal conductivity of air and ice at 271 and 203 K, respectively. Symbols correspond to the ICSSG [*Fierz et al.*, 2009].

The needle was heated with a constant power of 0.4 W m^{-1} once a day for 100 s, and the temperature rise in the middle of the needle was monitored and used to determine the apparent thermal conductivity $k^\star_{\text{needle}}$ relevant to this experimental approach [*Sturm et al.*, 1997; *Morin et al.*, 2010]. In parallel, the heat-flux at the bottom of the snow slab was measured continuously using two Hukseflux HFP01 sensors (accuracy of ±5 %), and divided by the temperature gradient measured using Pt100 temperature probes, to determine independently the vertical component of the apparent thermal conductivity of snow ($k^\star_z$).

3. Results

3.1. Effective Thermal Conductivity Versus Snow Density

[13] Figure 1 shows the two components k_z and k_{xy} of the effective thermal conductivity of snow, computed from all the 3D images considered in this work, as a function of snow density (ρ). Non-diagonal terms of $\mathbf{k}_{\text{eff}}$ are more than 100 times lower than diagonal terms and can be neglected (the image axes x, y and z correspond to the principal directions of the microstructure, z being along the direction of gravity and the macroscopic temperature gradient, which are similar in our cases). The figure shows that both components (k_z and k_{xy}) of $\mathbf{k}_{\text{eff}}$ are strongly correlated to snow density, and covary with it. The lowermost k_{eff} values are obtained for fresh snow, exhibiting values as low as 0.06 W m^{-1} K^{-1} ($k_z \simeq k_{xy}$) at a density of 103 kg m^{-3}. Refrozen wet snow shows the largest values, with k_{eff} values near 0.77 W m^{-1} K^{-1} at a density of 544 kg m^{-3}. The values of k_{eff} were fitted to snow density leading to the following equation:

$$k_{\text{eff}} = 2.5 \times 10^{-6}\rho^2 - 1.23 \times 10^{-4}\rho + 0.024 \quad (12)$$

[14] This fit has been chosen such as k_{eff} corresponds to the thermal conductivity of air when snow density is zero. The correlation coefficient for the 30 samples is 0.985,

which is best represented by the fact that standard deviation of the residuals to the regression curve is only 0.025 W m^{-1} K^{-1}. The regression curve is the same whether k_z or k_{eff} is used to derive equation (12). We also note that our data show an excellent agreement with the regression curve proposed by *Yen* [1981]: $k_{\text{eff}} = 2.22362 \times (\rho_{\text{snow}}/\rho_{\text{water}})^{1.885}$.

3.2. Anisotropy

[15] As displayed on Figure 1, several samples show a strong difference between the vertical and horizontal component of $\mathbf{k}_{\text{eff}}$. Rounded grains (RG) samples collected in the field, at a depth of several tens of cm below the surface, exhibit k_{xy} values higher than k_z. The ratio k_z/k_{xy} can be as low as 0.7. In contrast, several facetted (FC) and depth hoar (DH) samples exhibit an inverse behavior, where the k_z/k_{xy} ratio can be as high as 1.5. This anisotropy induces a slight scatter around the overall correlation between k_{eff} and ρ (equation (12)). We note that our anisotropy results are consistent with the recent study by *Shertzer and Adams* [2011], who estimated the effective thermal conductivity using microstructural parameters computed from 3D images. The granular approach used [*Batchelor and O'Brien*, 1977] was applied to two series of snow samples obtained during experiments under high temperature gradient. Although their computations are based on 2D slices of the full images and neglect heat conduction in air, the inception and build-up of anisotropy in terms of effective thermal conductivity of snow during temperature gradient metamorphism is in agreement with our results obtained on different snow types.

3.3. Influence of Temperature and Conduction in Interstitial Air

[16] In this section, for the sake of brevity, we focus on the vertical component k_z of $\mathbf{k}_{\text{eff}}$. However, the k_z results can be extended to the whole tensor $\mathbf{k}_{\text{eff}}$ without any loss of generality.

[17] Figure 2 shows that k_z increases with decreasing temperature in a non-linear manner depending on snow type. Although ice and air display opposite variations with temperature (k_{ice} increases while k_{air} decreases with decreasing temperature), this result indicates that much of the variations in $\mathbf{k}_{\text{eff}}$ stem from variations in k_{ice}. The effect is more pronounced in denser snow: snow with very high porosity, made mostly of air, shows almost no variation with temperature. Such results are opposite to the experimental findings of *Pitman and Zuckerman* [1967], who observed a decrease of $k^\star_z$ with decreasing temperature.

[18] The numerical experiments summarized in Table 1 demonstrate that conduction in interstitial air plays a vital role in heat transfer through snow. Indeed, ignoring heat

Table 1. Impact of Interstitial Air Conduction on the Effective Thermal Conductivity of Snow[a]

			k_z (W m^{-1} K^{-1})	
Sample	Type	ρ (kg m^{-3})	Air Conduction	No Air Conduction
I01	PP	103	0.06	0.006
I23	RG	256	0.16	0.10
4A	DH	315	0.25	0.18

[a]The absence of conduction in interstitial air was assessed by setting $k_{\text{air}} = 0$ W m^{-1} K^{-1}.

conduction in air leads to underestimating k_z by a factor 10 for precipitation particles (see Table 1). Even in denser snow such as depth hoar or rounded grains, neglecting conduction in air lowers by up to a factor 2 the effective thermal conductivity of snow. This result stems from the fact that, by setting k_{air} to zero, even the smallest gaps in the network of ice grains may lead to no heat transfer at all. The impact of dead-ends within the microstructure is therefore greatly enhanced when conduction in air is neglected. *Kaempfer et al.* [2005] carried out a simulation of k_z on a rounded grain snow sample with a density of 268 kg m^{-3}, held at 265 K, where they used a value for k_{ice} of 2.29 W m^{-1} K^{-1}. They found a value for k_z of 0.15 ± 0.01 W m^{-1} K^{-1}, by neglecting conduction in the pores. This value is consistent with our results, as it falls in between the two k_z values of one of our RG sample (see Table 1) featuring a similar density (256 kg m^{-3}), by taking into account, or not, heat conduction in interstitial air.

3.4. Comparison to Experimental Methods

[19] Figure 1 compares data from different methods to determine the effective or apparent thermal conductivity of snow, in the (k, ρ) space. Values of $\mathbf{k}_{eff}$ determined from 3D images are provided from *Kaempfer et al.* [2005] and this study. Data from needle-probe measurements ($k_{needle}^\star$) stem from the large compilation of *Sturm et al.* [1997], and also from measurements carried out during our own cold room experiment. Finally, data originating from experiments where the heat-flux and the temperature gradient were ratioed ($k_z^\star$) are given for our experiment and from *Kaempfer et al.* [2005]. The data indicate that, overall, the measurements from needle-probes are systematically significantly lower than other methods. Experimental data from flux/gradient measurements correspond better to k_z computations although discrepancies are also significant. We note that measurements by *Sturm et al.* [1997] and *Kaempfer et al.* [2005] were carried out at temperatures generally lower than the conditions of our simulations. Nevertheless, our results correspond to the upper bound of existing measurements, and computations carried out using conductive thermal properties of ice and air at lower temperatures indicate that $\mathbf{k}_{eff}$ components can only increase when temperature decreases. Neither the temperature dependency of k_{ice} and k_{air} nor the snow anisotropy explain the observed discrepancy.

4. Discussion and Conclusions

[20] *Riche and Schneebeli* [2010] have recently advocated that needle-probe measurements of the apparent thermal conductivity of snow ($k_{needle}^\star$) were biased low because of microstructural disturbances induced by the insertion of the needle into the snow. However, this conclusion was reached using an inadequate choice of instrumental parameters, in particular the heating time and the time window used to infer $k_{needle}^\star$. Indeed, numerical modeling of the impact of an air gap around the needle has shown no significant effect on the estimation of $k_{needle}^\star$, provided that the first 30 s into the heating period are discarded [*Morin et al.*, 2010]. Experiments on the same issue have ruled out that the quality of the thermal contact was a significant cause of error (M. Sturm, personal communication, 2011). However, in light of the discrepancy observed between the three available methods to measure the thermal properties of snow, it appears necessary to delve deeper into this conundrum. Firstly, it must be noted that the three methods (needle-probe, flux/gradient and numerical modeling) do not exactly probe the same variable. Needle-probe measurements are carried out under the assumption that the medium is homogeneous (i.e., the size of the REV is smaller than the typical radius of the cylinder of influence around the needle, i.e., about 10 mm in common snow types [*Morin et al.*, 2010]), isotropic (i.e., the vertical and horizontal components of $\mathbf{k}^\star$ are the same), and take place in transient mode, leading to the build-up of locally strong temperature gradients. Flux/gradient measurements focus only on the vertical component of $\mathbf{k}^\star$, in steady-state conditions. Last, as described above, numerical modeling considers only two out of the many processes potentially contributing to heat transfer in snow. It thus appears likely that the ability for the different techniques to provide convergent results strongly depends on snow type, and also on the temperature and the temperature gradient, as the latent heat effects and water vapor diffusion undoubtedly depend on these variables. Effects from snow type and temperature may even interact in a nontrivial manner. It also seems likely that the latent heat effects and water vapor diffusion contribute to heat transfer in variable proportions depending on snow type, given that k_z and $k_z^\star$ differ non systematically.

[21] In light of the above-mentioned findings, we recommend purely conductive effects (i.e., conduction through ice and interstitial air) to be considered separately from non-conductive processes. At present, the only method able to unambiguously characterize the purely conductive effective thermal conductivity is numerical modeling based on microstructure 3D images. Our study, carried out on 30 snow samples spanning the full range of seasonal snow type, reveals that the effective thermal conductivity of snow is strongly correlated with snow density, and follows closely the regression curve proposed by *Yen* [1981]. Unexpectedly, this corroborates the use of this relationship in several snowpack models (e.g., Crocus [*Brun et al.*, 1989]). Work is needed to disentangle the impact of non-conductive processes on experimental methods meant to determine $\mathbf{k}_{eff}$, as well as to better account for such effects in terms of heat transfer through the snowpack. An appealing approach is to explicitly simulate heat transfer in snow, taking into account both conductive and non-conductive effects, based on the microstructure of snow. Only at this cost will significant improvements of the understanding and modeling of heat transfer in snow occur.

References

Armstrong, R., and E. Brun (2008), *Snow and Climate: Physical Processes, Surface Energy Exchange and Modeling*, Cambridge Univ. Press, Cambridge, U. K.

Arons, E. M., and S. C. Colbeck (1995), Geometry of heat and mass transfer in dry snow: A review of theory and experiment, *Rev. Geophys.*, *33*, 463–493, doi:10.1029/95RG02073.

Auriault, J.-L. (1991), Heterogeneous medium. Is an equivalent description possible?, *Int. J. Eng. Sci.*, *29*(7), 785–795.

Auriault, J.-L., C. Boutin, and C. Geindreau (2009), *Homogenization of Coupled Phenomena in Heterogenous Media*, Wiley-ISTE, London.

Batchelor, G. K., and R. W. O'Brien (1977), Thermal and electrical conduction through a granular material, *Proc. R. Soc. London, Ser. A*, *355*, 313–333.

Bensoussan, A., J.-L. Lions, and G. Papanicolaou (1978), *Asymptotic Analysis for Periodic Structures*, North Holland, Amsterdam.

Brun, E., E. Martin, V. Simon, C. Gendre, and C. Coléou (1989), An energy and mass model of snow cover suitable for operational avalanche forecasting, *J. Glaciol.*, *35*(121), 333–342.

Brzoska, J.-B., C. Coléou, B. Lesaffre, S. Borel, O. Brissaud, W. Ludwig, E. Boller, and J. Baruchel (1999), 3D visualization of snow samples by microtomography at low temperature, *ESRF Newsl.*, *32*, 22–23.

Brzoska, J.-B., F. Flin, and J. Barckicke (2008), Explicit iterative computation of diffusive vapour field in the 3-D snow matrix: Preliminary results for low flux metamorphism, *Ann. Glaciol.*, *48*, 13–18.

Coléou, C., B. Lesaffre, J.-B. Brzoska, W. Ludwig, and E. Boller (2001), Three-dimensional snow images by X-ray microtomography, *Ann. Glaciol.*, *32*, 75–81, doi:10.3189/172756401781819418.

Domine, F., J. Bock, S. Morin, and G. Giraud (2011), Linking the effective thermal conductivity of snow to its shear strength and density, *J. Geophys. Res.*, doi:10.1029/2011JF002000, in press.

Fierz, C., R. Armstrong, Y. Durand, P. Etchevers, E. Greene, D. McClung, K. Nishimura, P. Satyawali, and S. Sokratov (2009), *The International Classification for Seasonal Snow on the Ground*, *Tech. Doc. Hydrol.*, vol. 83, UNESCO, Paris.

Flin, F., and J.-B. Brzoska (2008), The temperature gradient metamorphism of snow: Vapour diffusion model and application to tomographic images, *Ann. Glaciol.*, *49*, 17–21.

Flin, F., J.-B. Brzoska, B. Lesaffre, C. Coléou, and R. A. Pieritz (2003), Full three-dimensional modelling of curvature-dependent snow metamorphism: First results and comparison with experimental tomographic data, *J. Phys. D. Appl. Phys.*, *36*(10A), A49–A54, doi:10.1088/0022-3727/36/10A/310.

Flin, F., J.-B. Brzoska, B. Lesaffre, C. Coléou, and R. A. Pieritz (2004), Three-dimensional geometric measurements of snow microstructural evolution under isothermal conditions, *Ann. Glaciol.*, *38*, 39–44, doi:10.3189/172756404781814942.

Flin, F., et al. (2011), On the computations of specific surface area and specific grain contact area from snow 3D images, in *Physics and Chemistry of Ice*, edited by Y. Furukawa, pp. 321–328, Hokkaido Univ. Press, Sapporo, Japan.

Kaempfer, T. U., and M. Plapp (2009), Phase-field modeling of dry snow metamorphism, *Phys. Rev. E*, *79*(3), 031502, doi:10.1103/PhysRevE.79.031502.

Kaempfer, T. U., M. Schneebeli, and S. A. Sokratov (2005), A microstructural approach to model heat transfer in snow, *Geophys. Res. Lett.*, *32*, L21503, doi:10.1029/2005GL023873.

Morin, S., F. Domine, L. Arnaud, and G. Picard (2010), In-situ monitoring of the time evolution of the effective thermal conductivity of snow, *Cold Reg. Sci. Technol.*, *64*(2), 73–80, doi:10.1016/j.coldregions.2010.02.008.

Pinzer, B. R., and M. Schneebeli (2009), Snow metamorphism under alternating temperature gradients: Morphology and recrystallization in surface snow, *Geophys. Res. Lett.*, *36*, L23503, doi:10.1029/2009GL039618.

Pitman, D., and B. Zuckerman (1967), Effective thermal conductivity of snow at −88°C, −27°C and −5°C, *J. Appl. Phys.*, *38*, 2698–2699.

Raymond, C., and K. Tusima (1979), Grain coarsening of water-saturated snow, *J. Glaciol.*, *22*(86), 83–105.

Riche, F., and M. Schneebeli (2010), Microstructural change around a needle probe to measure thermal conductivity of snow, *J. Glaciol.*, *56*(199), 871–876, doi:10.3189/002214310794457164.

Rolland du Roscoat, S., M. Decain, C. Geindreau, X. Thibault, and J.-F. Bloch (2008), Microstructural analysis of paper using synchrotron X-ray microtomography: Numerical estimation of the permeability and effective thermal conductivity, *Appita J.*, *61*(4), 286–290.

Schneebeli, M., and S. A. Sokratov (2004), Tomography of temperature gradient metamorphism of snow and associated changes in heat conductivity, *Hydrol. Processes*, *18*(18), 3655–3665, doi:10.1002/hyp.5800.

Shertzer, R. H., and E. E. Adams (2011), Anisotropic thermal conductivity model for dry snow, *Cold Reg. Sci. Technol.*, doi:10.1016/j.coldregions.2011.09.005, in press. (Additional information is available at htpp://www.sciencedirect.com/science/article/pii/S0165232X1100187X.)

Sturm, M., J. Holmgren, M. König, and K. Morris (1997), The thermal conductivity of seasonal snow, *J. Glaciol.*, *43*(143), 26–41.

Thoemen, H., T. Walther, and A. Wiegmann (2008), 3D simulation of macroscopic heat and mass transfer properties from the microstructure of wood fibre networks, *Compos. Sci. Technol.*, *68*(3–4), 608–616, doi:10.1016/j.compscitech.2007.10.014.

Yen, Y.-C. (1981), Review of the thermal properties of snow, ice and sea ice, *Tech. Rep. 81-10*, Cold Reg. Res. and Eng. Lab., Hanover, N. H.

N. Calonne, F. Flin, B. Lesaffre, and S. Morin, CEN/Météo-France, 1441 rue de la piscine, F-38400 Saint Martin d'Hères CEDEX, France. (frederic.flin@meteo.fr; samuel.morin@meteo.fr)

C. Geindreau and S. Rolland du Roscoat, 3S-R, Domaine Universitaire, BP53, 38041 Grenoble CEDEX 9, France.